JOURNAL OF THE ROYAL SOCIETY Interface

DNA and lipid bilayers: self-assembly and insertion

Syma Khalid, Peter J Bond, John Holyoake, Robert W Hawtin and Mark S.P Sansom

J. R. Soc. Interface 2008 **5**, 241-250
doi: 10.1098/rsif.2008.0239.focus

Interface focus

J. R. Soc. Interface (2008) **5**, S241–S250
doi:10.1098/rsif.2008.0239.focus
Published online 2 September 2008

DNA and lipid bilayers: self-assembly and insertion

Syma Khalid[1,4,*], Peter J. Bond[2,4], John Holyoake[3,4], Robert W. Hawtin[1] and Mark S. P. Sansom[4]

[1]*School of Chemistry, University of Southampton, Southampton SO17 1BJ, UK*
[2]*Max Planck Institute of Biophysics, Max-von-Laue-Street 3, Frankfurt am Main 60438, Germany*
[3]*Molecular Structure and Function, Hospital for Sick Children, Toronto, Ontario, Canada M5G LX8*
[4]*Department of Biochemistry, University of Oxford, Oxford OX1 3QU, UK*

DNA–lipid complexes are of biomedical importance as delivery vectors for gene therapy. To gain insight into the interactions of DNA with zwitterionic and cationic (dimyristoyltrimethylammonium propane (DMTAP)) lipids, we have used coarse-grained molecular dynamics simulations to study the self-assembly of DPPC and DPPC/DMTAP lipid bilayers in the presence of a DNA dodecamer. We observed the spontaneous formation of lipid bilayers from initial systems containing randomly placed lipids, water–counterions and DNA. In both the DPPC and DPPC/DMTAP simulations, the DNA molecule is located at the water–lipid headgroup interface, lying approximately parallel to the plane of the bilayer. We have also calculated the potential of mean force for transferring a DNA dodecamer through a DPPC/DMTAP bilayer. A high energetic barrier to DNA insertion into the hydrophobic core of the bilayer is observed. The DNA adopts a transmembrane orientation only in this region. Local bilayer deformation in the vicinity of the DNA molecule is observed, largely as a result of the DNA–DMTAP headgroup attraction.

Keywords: molecular dynamics; coarse grain; DNA; gene therapy

1. INTRODUCTION

Synthetic non-viral delivery agents have been the focus of considerable attention as DNA carriers for gene therapy. In particular, complexes of cationic lipids (CL) and DNA have been shown to aid the entry of DNA into cells (Ewert *et al.* 2004). However, full exploitation of such complexes as DNA carriers has been hampered, in part by the poor understanding of the nature of the interactions of DNA with lipids, and of the mechanisms by which DNA may enter cells. DNA has been shown to form particularly strong complexes with CL such as DMTAP. Moreover, strong DNA–CL complexes alone are not sufficient for gene transfer; once inside the cell, DNA release from complexes either before or after transport into the nucleus is critically important.

X-ray studies by Safinya *et al.* have demonstrated the spontaneous formation of DNA–CL complexes by the mixing of DNA, unsaturated zwitterionic lipids (often known as 'helper' lipids) and CL in an aqueous environment (Radler *et al.* 1997; Safinya 2001). The electrostatic attraction between the anionic DNA and the CL along with the entropic gain associated with the release of tightly bound counterions from CL and DNA are the driving forces for the formation of a complex. A variety of DNA–CL complex morphologies have been reported. These include a lamellar phase in which DNA monolayers are sandwiched between bilayers of neutral and CL, and an inverted hexagonal phase in which the DNA is encapsulated within inverse cylindrical micelles (Radler *et al.* 1997; Koltover *et al.* 1998). The preferred morphology is dependent upon, for example, the chemical nature of the neutral or helper lipids (Safinya 2001). While these studies have provided insights into the structure of these complexes at a molecular level, the process of DNA release from such complexes remains poorly characterized.

Since the first atomistic molecular dynamics (MD) simulation of a mixed lipid–DNA system (Bandyopadhyay *et al.* 1999), there have been attempts at various levels of granularity to investigate similar systems using MD and Monte Carlo simulations (Bandyopadhyay *et al.* 1999; Farago *et al.* 2006). Bandyopadhyay *et al.* (1999) performed atomistic MD simulations of a DNA dodecamer embedded within a mixed DMTAP/DMPC lipid bilayer. These simulations revealed the roles of zwitterionic and

*Author and address for correspondence: School of Chemistry, University of Southampton, Southampton SO17 1BJ, UK (s.khalid@soton.ac.uk).

Electronic supplementary material is available at http://dx.doi.org/10.1098/rsif.2008.0239.focus or via http://journals.royalsociety.org.

One contribution of 9 to a Theme Supplement 'Biomolecular simulation'.

Received 4 June 2008
Accepted 4 August 2008

cationic lipid headgroups in screening the phosphate group charges of the DNA backbone. However, the computational requirements for an atomistic treatment of an extended system limited the simulations to a duration of only 4 ns. In the only other reported atomistic MD simulation of a DNA–lipid system, an external electric field was applied to drive the migration of a duplex DNA dodecamer across a zwitterionic lipid bilayer (Tarek 2005). Upon subjection to a transverse electric field, the DNA migrated into the bilayer core from its initial position at the lipid headgroup–water interface. While these simulations were able to provide valuable information about the DNA–lipid interactions, once again the computational demands of such a study did not allow exploration of the migration of the DNA duplex from one side of the bilayer to the other.

Coarse-grained (CG) treatments enable the simulation of large biological systems including DNA (Tepper & Voth 2005) and membranes (Venturoli *et al.* 2006; Reynwar *et al.* 2007). Such approaches have also been successfully applied to the study of DNA–CL complexes (Farago *et al.* 2006; Farago & Gronbech-Jensen 2007). CG models vary substantially in their level of granularity. For example, the number of particles used to represent a lipid molecule varies from two or three particles in mesoscale approaches (Reynwar *et al.* 2007) to approximately 12 particles (Shelley *et al.* 2001; Marrink *et al.* 2004; Nielsen *et al.* 2004; Shih *et al.* 2006). In the latter approach, groups of atoms are represented by spherical particles that interact via effective potentials. For example, in the CG model developed by Marrink *et al.* (2004), three to four particle types are used to represent phospholipids with an additional particle type representing a water molecule. To date, CG models of DNA–CL complexes have been more approximate. For example, solvent-free CG methods in which hydration is represented implicitly have been used to simulate the self-assembly of DNA–CL complexes (Farago *et al.* 2006; Farago & Gronbech-Jensen 2007). These simulations provided insights into the dependence of DNA chain spacing on the concentration of CLs and were in excellent agreement with experimental data. However, the reduced number of particles in the DNA and lipid models (three particles per lipid and DNA modelled as a rigid rod) did not allow discrimination between different types of lipid–DNA interactions, e.g. lipid–DNA backbone or lipid–DNA base interactions.

In summary, computational studies of DNA–CL complexes have either been at an atomic level of detail, and thus too short to study the self-assembly process, or been based on CG models that have not allowed the detailed study of the lipid–DNA interactions important in complex formation. The CG approach has been particularly hampered by the lack of a reduced particle DNA model that distinguishes between DNA phosphates, sugars and bases and is consistent in its mapping of atoms to particles with existing CG force fields for lipids and proteins. To the best of our knowledge, there are no reported simulation studies of the process of DNA release from DNA–CL complexes. Here, we have used a CG force field that bridges the atomistic and CG levels of granularity described above

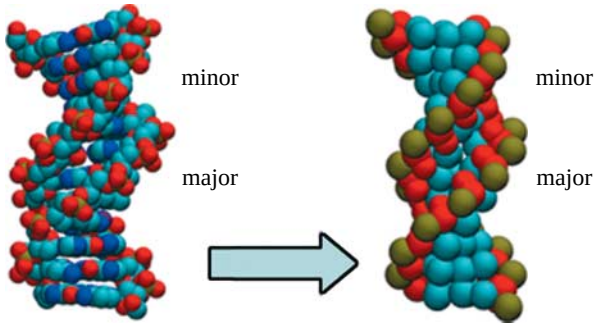

Figure 1. (*a*) Atomistic to (*b*) CG mapping. In the atomistic representation, the oxygen, nitrogen, carbon and phosphorus atoms are shown in red, blue, cyan and gold, respectively. In the CG model, the phosphate, sugar and base particles are shown in gold, red and cyan, respectively.

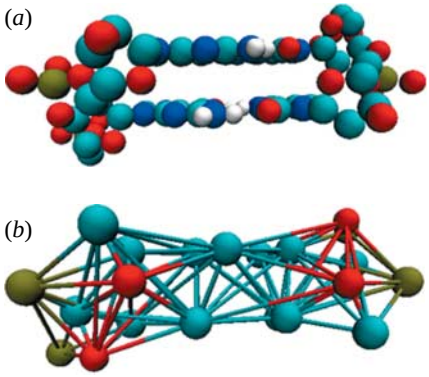

Figure 2. A ball-and-stick representation of two base pairs, viewed from the side. (*a*) In the atomistic model, the hydrogen, oxygen, nitrogen, carbon and phosphorus atoms are shown in white, red, blue, cyan and gold, respectively. (*b*) In the CG model, the phosphate, sugar and base particles are shown in gold, red and cyan, respectively. The lines connecting the particles represent the elastic network.

to perform simulations of large systems. The force field was developed to explore lipid and detergent dynamics and has more recently been used to study protein–lipid systems (Bond & Sansom 2006; Bond *et al.* 2007; Scott *et al.* 2008)

We have performed self-assembly simulations of a DNA dodecamer in DPPC and mixed DPPC/DMTAP lipid bilayers. Gene delivery via DNA–CL complexes relies not only upon the formation of the complex but also upon its dissociation to release the DNA once inside the cell, so that the DNA can migrate towards the cell nucleus. Thus, an understanding of DNA–lipid interactions and the barriers to DNA transfer through the complex are of interest. To this end, we have calculated the potential of mean force (PMF) for transferring a DNA dodecamer through a DPPC/DMTAP bilayer.

2. MODELS, SYSTEM SET-UP AND SIMULATION DETAILS

2.1. CG models

Simulations were performed using a CG representation of the components of the system. For the lipid molecules,

Table 1. Summary of the particle types that constitute the CG DNA model.

DNA component	number of particles	particle type		
phosphate	1	Qa		
deoxyribose sugar	2	C	Na	
adenine	3	Na	Na	Nda
thymine	2	Nda	Na	
guanine	3	Nda	Nda	Na
cytosine	2	Nd	Na	

we used the parameters developed by Marrink (Marrink *et al.* 2004). In this approach, approximately four heavy (i.e. not H) atoms are represented by a single particle. Water molecules are represented by a single particle as are Na^+ and Cl^- ions. Four particle types are distinguished by the force field. These are 'polar' (P), 'mixed polar/apolar' (N), 'hydrophobic apolar' (C) or 'charged' (Q) groups; further subtypes for the N and Q particles are included to allow fine tuning of the Lennard-Jones (LJ) interactions which in turn reflect hydrogen bonding capacities. Our model of DNA is built from these same four particle types. We used one particle for the phosphate group, two for the deoxyribose sugar and two and three for the pyrimidine and purine bases, respectively; the particles were chosen to reflect the chemical nature of the groups of atoms they represent (figure 1).

2.2. Non-bonded interactions

The non-bonded interactions between the CG particles are described by a 6–12 LJ potential. In all cases, the same effective LJ particle diameter of 0.47 nm is used. Five levels of LJ interaction are defined (Marrink *et al.* 2004). They range from attractive (representing strong polar interactions, P particles) through intermediate (representing non-polar interactions in aliphatic chains, N particles) to repulsive interactions (representing hydrophobic repulsion between polar and non-polar phases, C particles). Charged (Q) groups also interact via the standard coulombic potential with a relative dielectric constant of 20. Shift functions are applied so that energies and forces vanish at the cut-off distance. LJ interactions are smoothly shifted to zero between 0.9 and 1.2 nm. Coulombic interactions are also shifted to zero from 1.2 nm. The appropriate particle types were assigned according to partial charge and hydrogen bonding capacities of the constituent atoms of DNA nucleotides. Particle subtypes for Q and N particles are defined as in Marrink *et al.* (2004): 0 (no hydrogen bonding), d (hydrogen bonding donor), a (hydrogen bonding acceptor) or da (hydrogen bonding donor and acceptor), where, for example, Nda would be a non-polar particle with hydrogen bond acceptor and donor capabilities. Particle types used for the DNA model are summarized in table 1.

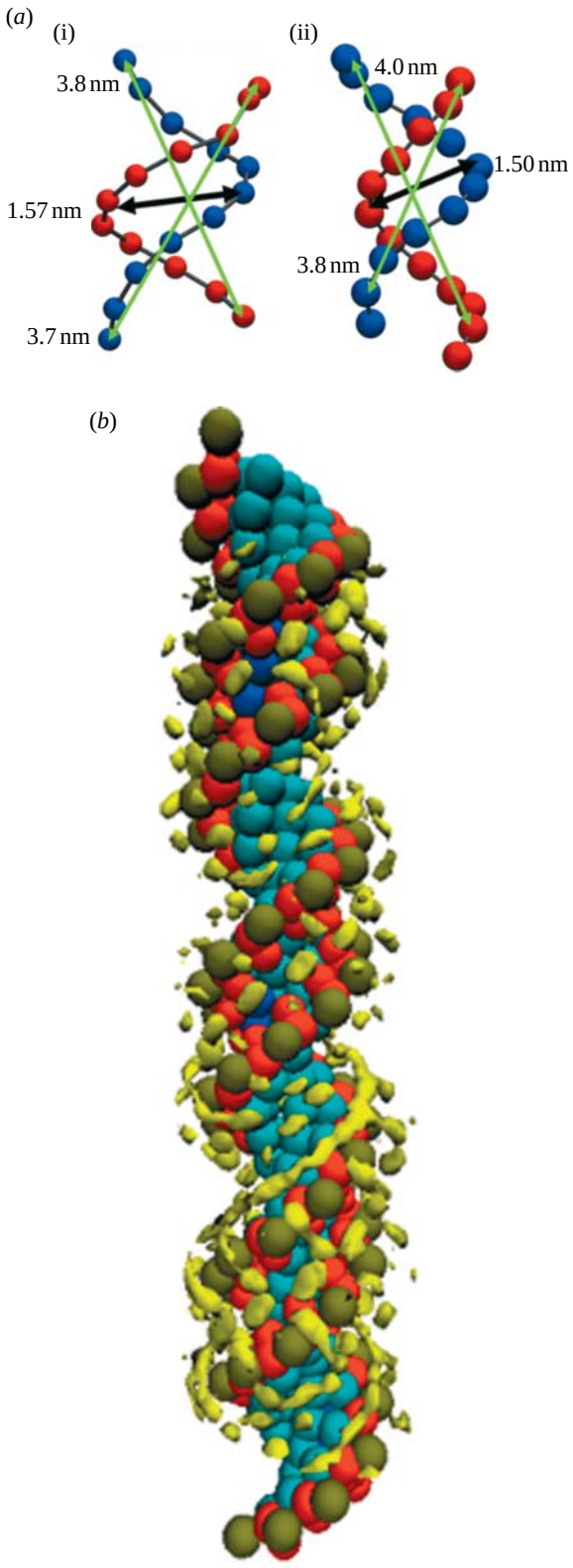

Figure 3. (*a*) Space-filling representation of phosphate atoms (i) in the X-ray structure of the DNA dodecamer $d(CGCGAATTCGCG)_2$ (pdb code 1BNA; Drew *et al.* 1981) and (ii) in the CG DNA after 30 ns of simulation. The end-to-end distances and groove width indicate the close agreement of our model with the X-ray structure. (*b*) Regions of high Na^+ density around the DNA 36mer obtained by superimposing approximately 15 000 configurations from a 200 ns trajectory and mapping the Na^+ density to a 0.1 nm grid. The Na^+ density is shown in yellow surface representation and the DNA is coloured as in figure 1.

Table 2. Summary of self-assembly simulations.

simulation name	system composition (+water and counterions)	simulation length (ns)	simulation details
^{DNA}DPPC	DNA and DPPC	50	self-assembly of bilayer
^{DNA}DPPC/DMTAP	DNA, DPPC and DMTAP	90	self-assembly of bilayer

2.3. Bonded interactions

The DNA-bonded interactions are based on an elastic network approach (Bahar *et al.* 1997; Atilgan *et al.* 2001). All particles within 0.7 nm of each other are connected by harmonic restraints with a 1500 kJ mol^{-1} nm^2 force constant (figure 2). Particles separated by more than 0.7 nm interact only via LJ and coulombic interactions. The equilibrium bond lengths are based on canonical B-form DNA molecules built with the nucleic acid builder module in Quanta (Accelrys Inc., San Diego, CA, USA).

2.4. Simulation protocols

All simulations were performed with the GROMACS 3.3.1 simulation package (www.gromacs.org; Berendsen *et al.* 1995; Lindahl *et al.* 2001). The neighbour list was updated every 10 steps. All simulations were performed at constant temperature, pressure and number of particles. The temperatures of the protein, DMTAP/DPPC lipids and solvent were coupled separately using the Berendsen algorithm at 323 K, with a coupling constant $\tau_T = 1$ ps (Berendsen *et al.* 1984). The system pressure was anisotropically coupled using the Berendsen algorithm at 1 bar with a coupling constant $\tau_P = 1$ ps and a compressibility of 1×10^{-5} bar^{-1}. The integration time step was 10 ps. Analyses were performed using GROMACS tools and locally written code. Rasmol and VMD were used for visualization (Sayle & Milner-White 1995; Humphrey *et al.* 1996).

2.5. Simulation details

The simulations of DNA with a single lipid species bilayer (^{DNA}DPPC) consisted of a DNA dodecamer, d(CCCCCTTTTTCC)$_2$, 256 DPPC lipids, 3176 water particles and 36 Na^+ particles. The simulations with a mixed lipid bilayer (^{DNA}DPPC/DMTAP) employed a system consisting of one DNA dodecamer, d(CCCCCTTTTTCC)$_2$, 116 DPPC lipids, 116 DMTAP lipids, 3073 water particles and 136 Cl^- particles. In each simulation, just enough counterions were added to ensure electroneutrality. All simulations were of 30–50 ns duration and were repeated twice to ensure reproducibility of results. Details of the system components for each simulation are given in table 2.

The PMF was calculated by performing a series of umbrella sampling simulations, which were then subjected to the weighted histogram analysis method (WHAM) for unbiasing. Starting configurations for each window of the umbrella sampling simulations were generated by superimposition of the DNA dodecamer into the centre of a pre-assembled DPPC/DMTAP lipid bilayer. The lipid bilayer contained 120 DPPC and 110 DMTAP lipids (with an equal distribution) in each leaflet. The centre of mass of the DNA was harmonically restrained to subsequent positions, each separated by $\Delta z = 0.2$ nm, along the bilayer normal, with a restraining force of 1000 kJ mol^{-1} nm^{-2}. Fifty windows were used with limits of +5.2 and −4.6 nm with respect to the bilayer centre, ensuring good sampling into the bulk solvent region. Prior to simulation, each window system was subjected to less than 500 steps of steepest descents energy minimization to remove any steric conflicts between the DNA, lipids and solvent. Each window simulation was equilibrated for 5 ns prior to a production run of 20 ns. Histograms were unbiased using WHAM with 200 bins and a tolerance of 10^{-5} kT for window offsets. PMFs were converged with respect to those variables, and to the number of simulation windows and equilibration time. PMF curves calculated over the first and second halves of equilibrated simulations overlapped. Error bars for each PMF window represent the difference between these two halves.

2.6. Time scales

The potential functions in the CG model are smoother than their atomistic counterparts, and thus the dynamics of the CG model are likely to be faster. However, the interpretation of the time scale in CG simulations is not straightforward. For example, it is possible to scale the time scale on the basis of comparison of diffusion coefficients for different system components with all-atom simulations. In our CG simulations, as in Marrink *et al.* (2004), the three-dimensional diffusion of water and the lateral diffusion of DPPC lipids are three to five times faster than those in the corresponding atomistic simulations. However, it is not possible to calibrate the dynamics of the DNA molecule or the DMTAP lipids since no equivalent atomistic simulations are currently available. As suggested by related CG studies of membrane–protein systems (Bond & Sansom 2006), coarse graining may be expected to speed up different dynamic processes to different extents. For these reasons, we have chosen not to rescale simulation times when presenting and interpreting our results. However, the reader should note that the motions of molecules presented here are likely to be significantly faster than when described in fully atomistic detail, with an upper limit of approximately an order of magnitude in relative scaling.

3. RESULTS

3.1. Validation of the DNA model

Simulations of DNA duplexes (300 base pairs) in water and counterions were used to validate our DNA model. DNA persistence lengths were estimated using the relationship

$$L_p = l_0/(1 - \langle \cos\theta \rangle),$$

where L_p is the calculated persistence length; l_0 is the average P–P distance; and θ is the backbone P–P–P angle (Cognet *et al.* 1999; Cifra 2004).

The values of approximately 49.0 nm estimated from our simulations correspond to approximately 148 base pairs and are in excellent agreement with experimentally determined persistence lengths of duplex DNA (approx. 150 base pairs; Hagerman 1988). Figure 3*a* indicates that the DNA end-to-end distance and groove widths (based on phosphate–phosphate distances) averaged over 30 ns of the simulation are in close agreement with the X-ray structure of the DNA dodecamer d(CGCGAATTCGCG)$_2$ (pdb code 1BNA) (Drew *et al.* 1981). We examined the behaviour of ions around the DNA from longer simulations of DNA 36mers (above 200 ns) in various NaCl concentrations. In agreement with atomistic simulations, we observed the association of the Na^+ ions with the DNA backbone, with some ion penetration (Na^+–base particle distance <0.8 nm) into the grooves (figure 3*b*; McConnell & Beveridge 2000; Rueda *et al.* 2004; Varnai & Zakrzewska 2004). Investigation of the sequence-dependent penetration of Na^+ ions into the minor groove (i.e. preference for AT-rich regions) reported in some atomistic simulations is beyond the scope of the current CG DNA model.

3.2. Self-assembly simulations

The self-assembly of the DPPC and binary mixture of DPPC/DMTAP lipids into bilayers in the presence of DNA proceeded via a mechanism similar to that reported previously for lipids in the presence and absence of membrane proteins (Marrink *et al.* 2004; Bond & Sansom 2006; Bond *et al.* 2007). The lipids form a continuous lamellar phase within the first few nanoseconds, which results in the burial of exposed hydrophobic lipid tails (figure 4). This is accompanied by the interaction of primarily one end of the DNA molecule, specifically the phosphate particles, with nearby choline and, in the case of DPPC, phosphate lipid particles. Both the DMTAP and DPPC headgroups contact the DNA approximately equally. An elongated lipid 'stalk' composed of both DMTAP and DPPC is observed bridging the bilayer and its periodic image after approximately 5 ns, which subsequently transforms into a bilayer-like structure during the next 5 ns. During this stage, one face of the DNA molecule interacts with nearby lipid headgroups. Thus, upon bilayer formation, the DNA is located at the water–lipid headgroup interface orientated such that it is lying along the bilayer plane, to maximize interactions between the anionic DNA backbone and the cationic DMTAP headgroups. This location of the DNA at the interfacial region of the membrane is subsequently maintained over further tens of nanoseconds. While the DNA molecule remains at the interfacial region, its interactions with the lipid headgroups do not prevent lateral motion; in fact, its centre of mass varies by up to approximately 2 nm along the x and y dimensions (parallel to the plane of the bilayer) throughout the simulation, relative to its initial bound position. Spontaneous insertion of the DNA into the non-polar acyl region of the bilayer is *not* observed.

The density profile of the ^{DNA}DPPC/DMTAP self-assembly simulation during the final 30 ns of the simulation (figure 5) shows the equilibrium densities (number of particles per unit volume) of the various system components in the z-direction (bilayer normal). The DNA molecule is positioned at the water–lipid headgroup interface. Interestingly, the positions of the DPPC and DMTAP headgroups in relation to the DNA molecule appear to be remarkably similar. The heights of the DPPC and DMTAP density peaks differ slightly as the headgroups are composed of different numbers of particles. Visual inspection and the density profile (figure 5) indicate approximately equal interaction of the two types of lipid with the DNA backbone phosphates. To investigate this further, we have decomposed the interaction of the DPPC headgroup with the DNA phosphate to consider the choline (NC3) and phosphate (PO4) groups separately. We have calculated radial distribution functions (RDFs) of both NC3 and PO4 groups and compared these to the DNA–DMTAP RDFs (figure 6). Spatial distribution functions (SDFs) that are not radially averaged were also calculated to show the distribution of lipids and water around the DNA nucleotides (figure 6). These show the DPPC and DMTAP molecules to be approximately evenly distributed around one face of the DNA, while the water molecules interact mainly with the opposite face.

The overall shape of the DNA–DMTAP choline and DNA–DPPC choline RDFs is almost identical, indicating that the equilibrium distance of the positively charged choline groups to the DNA phosphates corresponds almost exactly to the DMTAP choline groups. Overall, the height of the first peak is always slightly higher for the DNA–DMTAP RDF. By contrast, the RDF for the DNA–DPPC phosphate has a maximum corresponding to the second solvation shell of the DNA phosphate particles. For the DPPC and DMTAP headgroups to interact approximately equally with the DNA and be evenly distributed around one face of the DNA (figure 6), they would also have to interact with each other. Such an interaction would require a reorientation of the DPPC P^-–N^+ headgroup dipole to enable the DMTAP choline to interact with the DPPC phosphate group. NMR studies have shown that while the P^-–N^+ dipole of pure phospholipid bilayers remains approximately parallel to the bilayer normal, the addition of cationic amphiphiles results in a reorientation towards the water phase of approximately 30°. The angle made by the DPPC P^-–N^+ dipole with the bilayer normal varied between approximately 40° and 90° in the ^{DNA}DPPC simulations and had a mean angle of approximately $70 \pm 15°$. By contrast, the average angle fluctuated about a mean of approximately $60 \pm 2°$ in our 1 : 1 ^{DNA}DPPC/DMTAP simulations (see the electronic supplementary material, figure 1S). This is in qualitative agreement with the atomistic simulations of Bandyopadhyay *et al.* (1999),

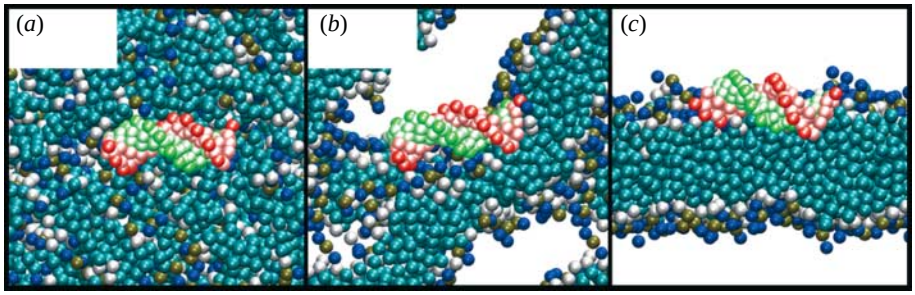

Figure 4. Space-filling representation of the formation of a lipid bilayer in the presence of a DNA molecule. (*a*) Randomly placed lipids around a DNA dodecamer (0 ns), (*b*) the formation of a lamellar phase (1 ns) and (*c*) DNA located at the lipid headgroup–water interface (30 ns). Water particles are omitted for clarity. Lipid tails are cyan and DNA strands are red and green with the backbone coloured darker than the bases.

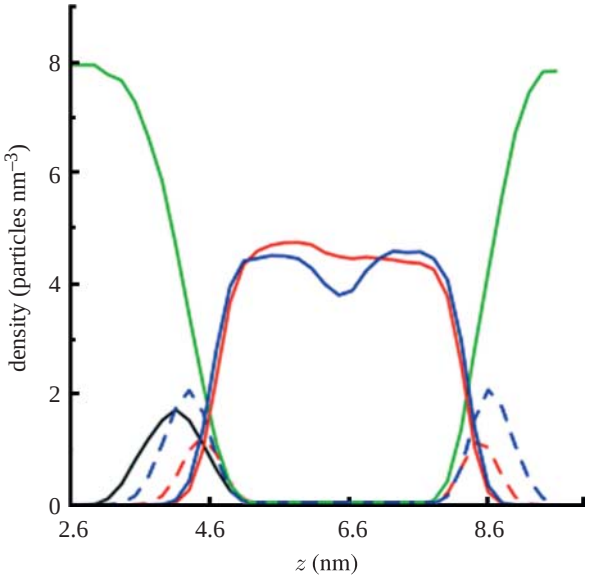

Figure 5. Density profile of the DMTAP/DPPC self-assembly simulation averaged over the last 30 ns of the simulation. Black, DNA; green, water; red, DMTAP; blue, DPPC. For both lipids, tails are represented by solid lines and headgroups by dashed lines.

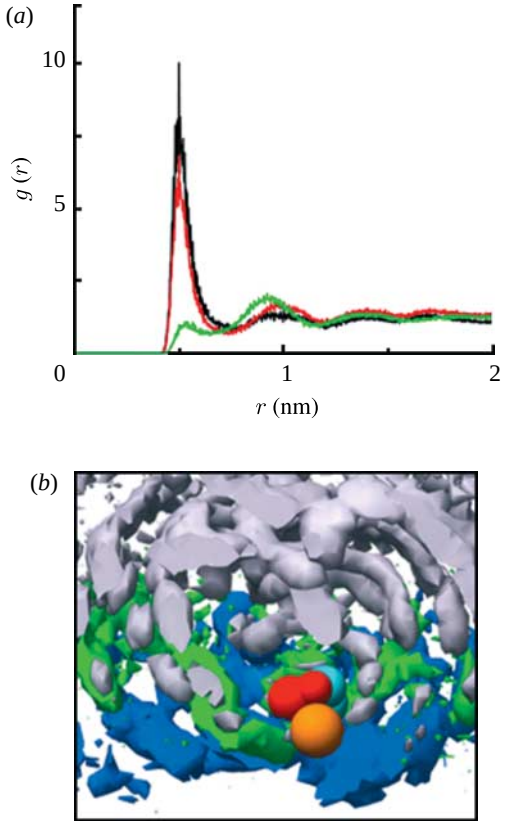

Figure 6. Interactions of DNA with lipid/water. (*a*) RDF between DNA phosphates and DMTAP choline (black), DPPC choline (red) and DPPC phosphate (green) groups. (*b*) SDF of water and lipids around a DNA nucleotide, representing water (grey), DMTAP headgroups (blue), DPPC headgroups (green), phosphate particles (orange), sugar particles (red) and DNA base particles (cyan).

which showed a close association of both cationic and zwitterionic headgroups with the DNA phosphate groups, made possible by a reorientation of the DMPC P^-–N^+ dipole. The larger range of angles in the ^{DNA}DPPC simulation indicates greater motion of the lipid headgroups, while in the presence of DMTAP, the range of angles between the P^-–N^+ dipole and the bilayer normal is much narrower; this is suggestive of tighter packing between the DPPC and DMTAP headgroups compared with the pure DPPC lipid bilayer.

Lipid–lipid RDFs show a slightly higher probability of finding a DMTAP choline group within the first solvation shell of a DPPC phosphate group than a DPPC choline (see the electronic supplementary material, figure 2S). The tight headgroup packing in the DMTAP/DPPC mixture is further confirmed by the value of 61 ± 0.5 Å^2 for the area per lipid calculated from the equilibrated portion of our simulations, which is similar to the value of 63 ± 0.5 Å^2 calculated for the ^{DNA}DPPC system. These observations are in agreement with the atomistic simulations of Gurtovenko & Vattulainen (2005) and experimental studies of Zantl *et al.* (1999), which showed similar tight packing of zwitterionic lipids and CL. Characterization of DNA–DMPC/DMTAP complexes by infrared spectroscopy has indicated strong interaction of Cl^- ions with the DMTAP headgroups, where the Cl^- ions are interdigitated between the lipid headgroups and shield the repulsion between positively charged TAP moeties; this effect is particularly important in the crystalline phase. Gurtovenko & Vattulainen (2005) reported almost identical RDFs for DMPC–Cl^- and DMTAP–Cl^-. Encouragingly, RDFs calculated from our simulations also indicate similar interaction between Cl^- ions

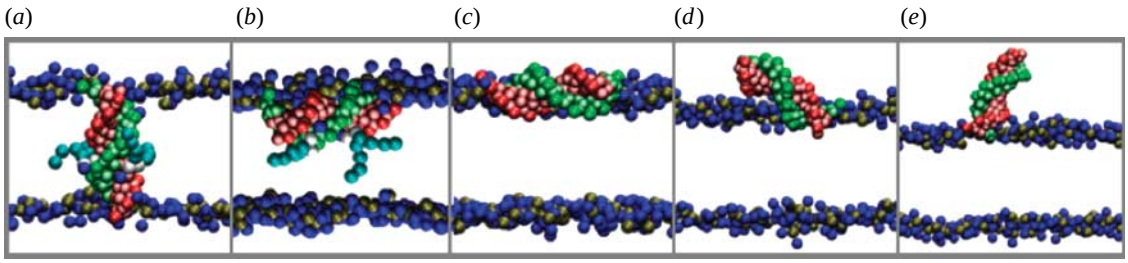

Figure 7. Representative simulation snapshots for different umbrella sampling windows, centred around $z=$(*a*) 0, (*b*) 1, (*c*) 2.4, (*d*) 3 and (*e*) 4 nm. The colour scheme for DNA is as in figure 4. The lipid DPPC and DMTAP headgroups are shown in space-filling format, with phosphate groups in brown and choline groups in blue. Selected DMTAP molecules whose headgroups have significantly penetrated the membrane core are shown in their entirety, with the glycerol backbone in white and lipid tails in cyan.

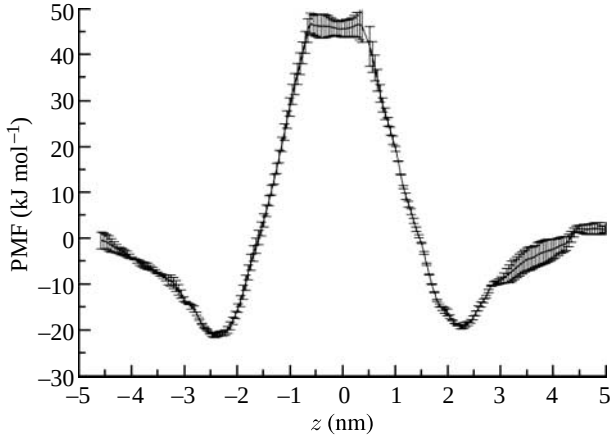

Figure 8. PMF for transfer of a DNA molecule across the normal (z) of a mixed DPPC/DMTAP bilayer and into the bulk solvent. Error bars represent the difference between PMFs calculated for the first and second halves of each simulation.

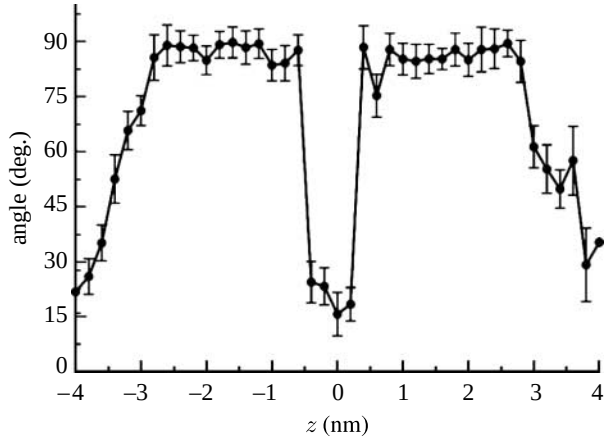

Figure 9. Average angle (calculated over the final 5 ns of each umbrella sampling window production run) between bilayer normal (z) and DNA long axis, calculated as a function of z. Error bars represent standard deviation over the 5 ns.

and both the DPPC and DMTAP headgroups (see the electronic supplementary material, figure 2S). It seems reasonable that as the DMTAP and DPPC headgroups interact almost equally with the DNA backbone phosphates, they would also both interact

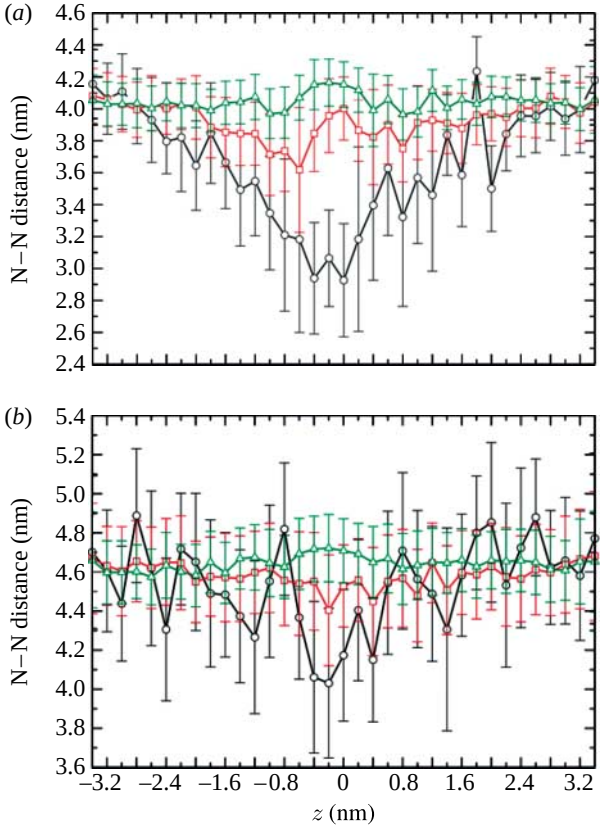

Figure 10. Local bilayer deformation of the bilayer for (*a*) DMTAP or (*b*) DPPC lipids as a function of z, indicated by the average distance (calculated over the final 5 ns of each umbrella sampling window production run) between upper- and lower-leaflet choline (N) particles (dNN) within 0.5 (black), 1.5 (red) and 2.5 nm (green) of the DNA molecule's centre of mass. Error bars represent standard deviation over the 5 ns.

similarly with Cl^- ions as the same number of charges is involved.

The DPPC–DNA system was neutralized by the addition of Na^+ ions. These ions show a marked preference for the DNA phosphate groups over the DPPC phosphate groups. Individual DNA–Na^+ interactions (DNA–$Na^+ \leq 0.8$ nm) are maintained over approximately 10 ps time scale, thus the ions are able to exchange with the solvent and interact with more than one phosphate particle along the DNA backbone over the time scale of the simulations.

3.3. PMFs via umbrella sampling

Experimental studies have shown that DNA–CL complexes feature strong DNA–lipid interactions with the DNA either sandwiched between lipid bilayers or encapsulated within inverse cylindrical micelles (Radler *et al.* 1997; Koltover *et al.* 1998). It is likely that the DNA–lipid interactions play a key role in the ability of DNA to escape from the DNA–CL complex once inside the cell. Calculating barriers to DNA transfer across lipid bilayers should help to identify the energetics associated with key DNA–lipid interactions that may be involved in the process of DNA escape from the complex. Thus, we calculated the PMF for transferring a DNA dodecamer through a DPPC/DMTAP bilayer (figure 7). Each leaflet was equally composed of DPPC and DMTAP molecules with a constant ratio of 12 : 11. The PMF was calculated via a series of 50 ns umbrella sampling simulations, during which the DNA centre of mass was restrained at positions separated by $\Delta z = 0.2$ nm along the bilayer normal, z.

As expected for a highly charged macromolecule, there is a large barrier (approx. 50 kJ mol^{-1} relative to the bulk solvent) to insertion of the DNA into the hydrophobic core of the bilayer between $z = -0.5$ and $+0.5$ nm (figures 7*a* and 8). In this region, the DNA molecule adopts a transmembrane orientation and significant local shrinking of the bilayer is observed (figure 9). Measurement of the mean distance between choline particles of the upper and lower leaflets revealed the local bilayer deformation to be primarily due to DNA–DMTAP attraction, with membrane shrinking of approximately 1 nm within 0.5 nm of the DNA centre of mass for DMTAP, but only approximately 0.5 nm for DPPC (figure 10*a*,*b*). While the DNA is in this region, a number of DMTAP headgroups in close association with the DNA backbone are observed to enter the hydrophobic tail region of the bilayer (figure 7*a*), thereby presumably reducing some of the energetic penalty incurred as the DNA phosphate particles are exposed to the hydrophobic core of the bilayer. Beyond $z \sim \pm 0.5$ nm on either side of the bilayer centre, the PMF barrier is overcome (figure 8), with the DNA molecule adopting an in-plane orientation relative to the z-axis (figure 9). This orientation presumably requires less bilayer deformation for the partial 'solvation' of the membrane-exposed DNA phosphate particles, although some DMTAP headgroups continue to associate with the DNA molecule within the hydrophobic core (figure 7*b*). Between $z \sim \pm 2.0$ and ± 2.5 nm, the system minimum energy state is obtained (figure 10), at the membrane interface region (figure 7*c*), with a well of approximately -20 kJ mol^{-1} relative to the bulk solvent, or approximately -70 kJ mol^{-1} relative to the hydrophobic membrane centre. Here, the bilayer deformation is no longer present (figure 10*a*). Finally, beyond $z \sim \pm 2.5$ nm, the boundary of the interfacial free-energy well is reached and the DNA partitions towards the bulk solvent (figure 7*d*,*e*). In this region, the DNA gradually loses the favoured in-plane orientation as one end of the molecule is pulled away from the membrane surface.

4. DISCUSSION

Our simulations have shown that self-assembly of lipids (either DPPC or DMTAP/DPPC) around a DNA dodecamer leads to the formation of lipid bilayers with the DNA molecule located at the bilayer–water interface. In agreement with earlier atomistic studies (Bandyopadhyay *et al.* 1999), we observe a reorientation of the DPPC headgroups that enables them to interact with the DNA backbone. Cl^- ions interact strongly with the headgroups of both lipid types. The PMF profile across a DPPC/DMTAP bilayer for a DNA dodecamer was calculated to identify DNA–lipid interactions that must be overcome when DNA is released from a DNA–CL complex. As expected, there is a relatively high energetic barrier to transferring the DNA across the hydrophobic acyl tail region of the bilayer. To minimize the exposure of the charged DNA backbone to the lipid tails, the DNA adopts a transmembrane orientation in this region. DNA–lipid headgroup attraction leads to the local deformation of the bilayer in the vicinity of the DNA. This is largely a result of DNA–DMTAP interactions. A number of DMTAP lipids (headgroups) enter the hydrophobic core of the bilayer while in close contact with the DNA phosphate particles, thus forming a DNA–lipid complex.

The high barrier experienced by the DNA molecule as it crosses the membrane core is unsurprising, given that it involves the transfer of multiple charged phosphates, along with accompanying polar headgroups. Even so, it is possible that the barrier height in the centre of the bilayer is underestimated. This is due to the simplicity of the CG force field (e.g. the water particles contain no dipole) and the deficiency in the treatment of electrostatics, with only short-range electrostatics and constant dielectric screening. Indeed, recent simulations (Bond *et al.* submitted; Monticelli *et al.* 2008) reveal that the free-energy barrier for insertion of a single CG charged particle into the centre of a membrane is around a third to a half lower than that estimated from all-atom simulations. On the other hand, PMF profiles across a membrane calculated for CG charged transmembrane peptides (Bond *et al.* submitted) have a shape similar to equivalent atomistic simulations, and exhibit comparable effects on the local membrane structure. Thus, it seems reasonable to expect that such a CG treatment for DNA as presented here should provide at least a semi-quantitative description for the interaction with the membrane. Further refinement in the CG model would benefit from a direct calibration of solvation or partition free energies of DNA molecules, but will require novel all-atom simulations and experiments.

The formation of the lipid–DNA complex in the centre of the membrane is in agreement with atomistic simulations and has been suggested by experimental studies (Bandyopadhyay *et al.* 1999; Golzio *et al.* 2002; Tarek 2005). To the best of our knowledge, there have not been any reported atomistic PMFs of DNA transfer

across a lipid bilayer with which to compare our results from CG simulations. However, PMF profiles of peptides (both charged and hydrophobic) across a DPPC bilayer calculated with CG force fields similar to that used here reveal a good correlation with atomistic simulations (Bond *et al.* submitted; Monticelli *et al.* 2008). While our CG model is unable to predict specific interactions, our simulations do indicate that cationic and zwitterionic lipids as well as ions play a key role in the formation of DNA–lipid complexes. Moreover, our results suggest that both the strength of the DNA–CL interaction and the orientation of the DNA molecule itself may influence the release of DNA from these complexes once they have crossed the membrane into cells. The high barrier to insertion of the DNA into the lipid bilayer suggests that the escape of the DNA from DNA–CL complexes does not involve DNA migrating through the lipid tail region. Instead, the mechanism by which DNA escapes may involve rearrangement of the lipid headgroups, perhaps to form a hydrophilic pore. The barrier to DNA transfer through such a pore would be much lower than that for transfer through the lipid tail region.

Looking beyond the present study, the calculation of PMFs with CG models such as the one described here can be used to predict the strength of DNA–lipid interactions, thus providing a useful predictive tool for the design of DNA–CL complexes for gene therapy. While DNA delivery into cells for gene therapy may concern much longer strands of DNA than the one considered in the present study, the CG-MD approach can be readily applied to much longer strands of DNA and will allow the study of larger systems that bridge the size gap between experiment and simulation.

We thank the BBSRC, EPSRC, Wellcome Trust, MRC and the Bionanotechnology IRC for funding. P.J.B. is an EMBO fellow. We thank G. Attard and P. Fowler for their helpful discussions.

REFERENCES

Atilgan, A. R., Durell, S. R., Jernigan, R. L., Demirel, M. C., Keskin, O. & Bahar, I. 2001 Anisotropy of fluctuation dynamics of proteins with an elastic network model. *Biophys. J.* **80**, 505–515.

Bahar, I., Atilgan, A. R. & Erman, B. 1997 Direct evaluation of thermal fluctuations in proteins using a single-parameter harmonic potential. *Fold Des.* **2**, 173–181. (doi:10.1016/S1359-0278(97)00024-2)

Bandyopadhyay, S., Tarek, M. & Klein, M. L. 1999 Molecular dynamics study of a lipid–DNA complex. *J. Phys. Chem. B* **103**, 10075–10080. (doi:10.1021/jp9927496)

Berendsen, H. J. C., Postma, J. P. M., van Gunsteren, W. F., DiNola, A. & Haak, J. R. 1984 Molecular dynamics with coupling to an external bath. *J. Chem. Phys.* **81**, 3684–3690. (doi:10.1063/1.448118)

Berendsen, H. J. C., van der Spoel, D. & van Drunen, R. 1995 GROMACS: a message-passing parallel molecular dynamics implementation. *Comput. Phys. Commun.* **95**, 43–56. (doi:10.1016/0010-4655(95)00042-E)

Bond, P. J. & Sansom, M. S. P. 2006 Insertion and assembly of membrane proteins via simulation. *J. Am. Chem. Soc.* **128**, 2697–2704. (doi:10.1021/ja0569104)

Bond, P. J., Holyoake, J., Ivetac, A., Khalid, S. & Sansom, M. S. 2007 Coarse-grained molecular dynamics simulations of membrane proteins and peptides. *J. Struct. Biol.* **157**, 593–605. (doi:10.1016/j.jsb.2006.10.004)

Bond, P. J., Wee, C. L. & Sansom, M. S. P. Submitted. Coarse-grained molecular dynamics simulations of the energetics of helix insertion into a lipid bilayer.

Cifra, P. 2004 Differences and limits in estimates of persistence length for semi-flexible macromolecules. *Polymer* **45**, 5995–6002. (doi:10.1016/j.polymer.2004.06.034)

Cognet, J. A. H., Pakleza, C., Cherny, D., Delain, E. & Le Cam, E. 1999 Static curvature and flexibility measurements of DNA with microscopy. A simple renormalization method, its assessment by experiment and simulation. *J. Mol. Biol.* **285**, 997–1009. (doi:10.1006/jmbi.1998.2322)

Drew, H. R., Wing, R. M., Takano, T., Broka, C., Tanaka, S., Itakura, K. & Dickerson, R. E. 1981 Structure of a B-DNA dodecamer—conformation and dynamics. 1. *Proc. Natl Acad. Sci. USA-Biol. Sci.* **78**, 2179–2183. (doi:10.1073/pnas.78.4.2179)

Ewert, K., Slack, N. L., Ahmad, A., Evans, H. M., Lin, A. J., Samuel, C. E. & Safinya, C. R. 2004 Cationic lipid–DNA complexes for gene therapy: understanding the relationship between complex structure and gene delivery pathways at the molecular level. *Curr. Med. Chem.* **11**, 133–149. (doi:10.2174/0929867043456160)

Farago, O. & Gronbech-Jensen, N. 2007 Computational and analytical modeling of cationic lipid–DNA complexes. *Biophys. J.* **92**, 3228–3240. (doi:10.1529/biophysj.106.096990)

Farago, O., Gronbech-Jensen, N. & Pincus, P. 2006 Mesoscale computer modeling of lipid–DNA complexes for gene therapy. *Phys. Rev. Lett.* **96**, 018102. (doi:10.1103/PhysRevLett.96.018102)

Golzio, M., Teissie, J. & Rols, M. P. 2002 Direct visualization at the single-cell level of electrically mediated gene delivery. *Proc. Natl Acad. Sci. USA* **99**, 1292–1297. (doi:10.1073/pnas.022646499)

Gurtovenko, A. A. & Vattulainen, I. 2005 Pore formation coupled to ion transport through lipid membranes as induced by transmembrane ionic charge imbalance: atomistic molecular dynamics study. *J. Am. Chem. Soc.* **127**, 17570–17571. (doi:10.1021/ja053129n)

Hagerman, P. J. 1988 Flexibility of DNA. *Ann. Rev. Biophys. Biophys. Chem.* **17**, 265–286. (doi:10.1146/annurev.bb.17.060188.001405)

Humphrey, W., Dalke, A. & Schulten, K. 1996 VMD—visual molecular dynamics. *J. Mol. Graph. Model.* **14**, 33–38. (doi:10.1016/0263-7855(96)00018-5)

Koltover, I., Salditt, T., Radler, J. O. & Safinya, C. R. 1998 An inverted hexagonal phase of cationic liposome–DNA complexes related to DNA release and delivery. *Science* **281**, 78–81. (doi:10.1126/science.281.5373.78)

Lindahl, E., Hess, B. & van der Spoel, D. 2001 GROMACS 3.0: a package for molecular simulation and trajectory analysis. *J. Mol. Model.* **7**, 306–317.

Marrink, S. J., de Vries, A. H. & Mark, A. E. 2004 Coarse grained model for semiquantitative lipid simulations. *J. Phys. Chem. B* **108**, 750–760. (doi:10.1021/jp036508g)

McConnell, K. J. & Beveridge, D. L. 2000 DNA structure: what's in charge? *J. Mol. Biol.* **304**, 803–820. (doi:10.1006/jmbi.2000.4167)

Monticelli, L., Kandasamy, S. K., Periole, X., Larson, R. G., Tieleman, D. P. & Marrink, S. J. 2008 The MARTINI coarse-grained force field: extension to proteins. *J. Chem. Theory Comput.* **4**, 819–834. (doi:10.1021/ct700324x)

Nielsen, S. O., Lopez, C. F., Ivanov, I., Moore, P. B., Shelley, J. C. & Klein, M. L. 2004 Transmembrane peptide-induced lipid sorting and mechanism of L_α-to-inverted

phase transition using coarse-grain molecular dynamics. *Biophys. J.* **87**, 2107–2115. (doi:10.1529/biophysj.104.040311)

Radler, J. O., Koltover, I., Salditt, T. & Safinya, C. R. 1997 Structure of DNA–cationic liposome complexes: DNA intercalation in multilamellar membranes in distinct interhelical packing regimes. *Science* **275**, 810–814. (doi:10.1126/science.275.5301.810)

Reynwar, B. J., Illya, G., Harmandaris, V. A., Muller, M. M., Kremer, K. & Deserno, M. 2007 Aggregation and vesiculation of membrane proteins by curvature-mediated interactions. *Nature* **447**, 461–464. (doi:10.1038/nature05840)

Rueda, M., Cubero, E., Laughton, C. A. & Orozco, M. 2004 Exploring the counterion atmosphere around DNA: what can be learned from molecular dynamics simulations? *Biophys. J.* **87**, 800–811. (doi:10.1529/biophysj.104.040451)

Safinya, C. R. 2001 Structures of lipid–DNA complexes: supramolecular assembly and gene delivery. *Curr. Opin. Struct. Biol.* **11**, 440–448. (doi:10.1016/S0959-440X(00)00230-X)

Sayle, R. A. & Milner-White, E. J. 1995 RasMol: biomolecular graphics for all. *Trends Biochem. Sci.* **20**, 374–376. (doi:10.1016/S0968-0004(00)89080-5)

Scott, K. A., Bond, P. J., Ivetac, A., Chetwynd, A. P., Khalid, S. & Sansom, M. S. 2008 Coarse-grained MD simulations of membrane protein-bilayer self-assembly structure. *Structure* **16**, 621–630.

Shelley, J. C., Shelley, M. Y., Reeder, R. C., Bandyopadhyay, S. & Klein, M. L. 2001 A coarse grain model for phospholipid simulations. *J. Phys. Chem. B* **105**, 4464–4470. (doi:10.1021/jp010238p)

Shih, A. Y., Arkhipov, A., Freddolino, P. L. & Schulten, K. 2006 Coarse grained protein–lipid model with application to lipoprotein particles. *J. Phys. Chem. B* **110**, 3674–3684. (doi:10.1021/jp0550816)

Tarek, M. 2005 Membrane electroporation: a molecular dynamics simulation. *Biophys. J.* **88**, 4045–4053. (doi:10.1529/biophysj.104.050617)

Tepper, H. L. & Voth, G. A. 2005 A coarse-grained model for double-helix molecules in solution: spontaneous helix formation and equilibrium properties. *J. Chem. Phys.* **122**, 124 906. (doi:10.1063/1.1869417)

Varnai, P. & Zakrzewska, K. 2004 DNA and its counterions: a molecular dynamics study. *Nucleic Acids Res.* **32**, 4269–4280. (doi:10.1093/nar/gkh765)

Venturoli, M., Maddalena Sperotto, M., Kranenburg, M. & Smit, B. 2006 Mesoscopic models of biological membranes. *Phys. Rep.* **437**, 1–54. (doi:10.1016/j.physrep.2006.07.006)

Zantl, R., Baicu, L., Artzner, F., Sprenger, I., Rapp, G. & Rädler, J. O. 1999 Thermotropic phase behavior of cationic lipid–DNA complexes compared to binary lipid mixtures. *J. Phys. Chem.* **103**, 10 300–10 310.